



Cite this: DOI: 10.1039/c6ce00749j

# 1,2,4-Triazole-based molecular switches: crystal structures, Hirshfeld surface analysis and optical properties†

Damir A. Safin, Koen Robeyns and Yann Garcia\*

We have studied a series of eight closely related *N*-salicylidene-4-amino-1,2,4-triazole molecules 1–8, obtained by condensation of the corresponding aldehyde with 4-amino-4*H*-1,2,4-triazole. <sup>1</sup>H NMR spectroscopy in solution revealed the presence of a single structure at least in DMSO-*d*<sub>6</sub>. According to single-crystal X-ray diffraction, it was established that the crystal structures of 5–8 each are stabilized by a linear intramolecular hydrogen bond of the O–H⋯N type, formed between the *o*-OH hydrogen atom of the phenolic ring and the imine nitrogen atom. The same *o*-OH function in the crystal structures of 1–4 was found to be involved in the intermolecular hydrogen bonds with one of the triazole nitrogen atoms of the adjacent molecule. The overall geometry of each molecule in the structures of 1–8 was found to be almost planar or slightly deviated from planarity. Hirshfeld surface analysis showed that the structures of all compounds are mainly characterized by H⋯H, H⋯C, H⋯N and H⋯O contacts but some contribution from C⋯C and C⋯N contacts is also clearly observed. Diffuse reflectance spectroscopy reveals the exclusive presence of the enol form in the solid state at room temperature for 1–6 and 8, while a mixture of dominant enol and *cis*-keto forms were found for 7. All the studied molecules 1–8 were not photo-switchable, while 7 was found to be thermochromic from coloured to colourless upon cooling.

Received 3rd April 2016,  
Accepted 20th May 2016

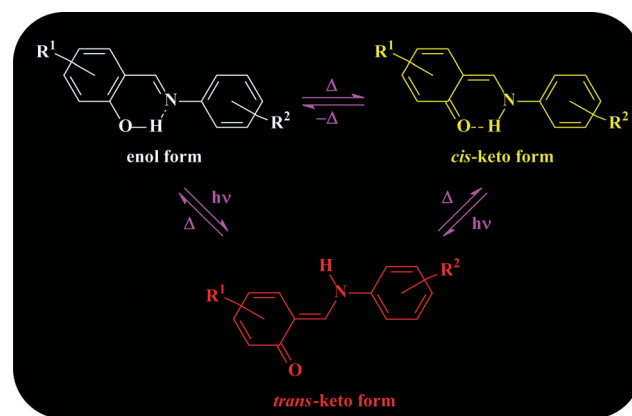
DOI: 10.1039/c6ce00749j

www.rsc.org/crystengcomm

## Introduction

Optical devices are of great importance due to their considerable and leading role in both daily life and instrumentation.<sup>1</sup> Chromism-based molecular switches seem to be the most attractive ones because of the smart and controlled change of their chromic properties. Among them solid state thermo- and photochromic compounds are considered the most relevant working mass for smart devices.<sup>2</sup> *N*-Salicylidene aniline derivatives (Scheme 1), as well as their *N*-heterocyclic analogues, dominate over other classes of molecules, exhibiting thermo- and photochromic molecules in the crystalline state.<sup>3</sup> This is explained by both their colour panel and their accessible forms (Scheme 1) as well as ease of synthesis due to Schiff base condensation.<sup>4</sup> Another advantage of *N*-salicylidene aniline derivatives, making them attractive from a synthetic point of view, is the possibility of being included into various matrices to form hybrid materials<sup>5</sup> and blends.<sup>6</sup>

The solid state thermochromic properties of *N*-salicylidene aniline derivatives were first considered to result from the planarity of the molecule and the formation of a “close-packed crystal structure” (dihedral angle between the aromatic rings  $\phi < 25^\circ$ ), whereas photochromic behaviour is caused by the significant rotation of aromatic rings and the formation of an “open structure” ( $\phi > 25^\circ$ ).<sup>4,5</sup> Thermo- and photochromic properties were stated over the years to be mutually exclusive.<sup>4b</sup> A number of contradicting examples showing both thermo- and photochromic properties have,



Scheme 1

Institute of Condensed Matter and Nanosciences, Molecules, Solids and Reactivity (IMCN/MOST), Université catholique de Louvain, Place L. Pasteur 1, 1348 Louvain-la-Neuve, Belgium. E-mail: yann.garcia@uclouvain.be; Fax: +32 1047 2330; Tel: +32 1047 2831

† Electronic supplementary information (ESI) available: Additional data, Fig. S1–S8 and Tables S1–S3. CCDC 1451196–1451202. For ESI and crystallographic data in CIF or other electronic format see DOI: 10.1039/c6ce00749j

however, been recently discovered.<sup>5b,7,8</sup> All these newly obtained examples demonstrated that it is not possible to explain the thermo- and photochromism of *N*-salicylidene aniline derivatives solely based on their crystal structures, but energy differences between ground and excited states need also to be considered.<sup>5b</sup> Furthermore, a complete and detailed crystal structure analysis, including  $\phi$ , crystal packing and the available free space around the switching unit in addition to the flexibility of the nearby environment, is necessary.<sup>8</sup> All this is obviously dictated by a diversity of noncovalent intermolecular interactions responsible for the overall crystal packing of molecules.<sup>9</sup>

The thermo- and photochromic properties of a great number of mono-*N*-salicylidene aniline derivatives as well as several bis(salicylidene) and tris(salicylidene) derivatives have been thoroughly studied.<sup>4–8,10</sup> In continuation of our comprehensive studies of *N*-salicylidene aniline derivatives and with the aim of understanding their structural features, which influence their optical properties, we have directed our attention to a series of eight closely related *N*-salicylidene-4-amino-1,2,4-triazole-based molecules modified by their *N*-salicylidene fragment (Chart 1). Among them only the crystal structure and optical properties of *N*-salicylidene-4-amino-1,2,4-triazole, **1** (Chart 1), have been studied so far.<sup>7a</sup> This is really surprising given that iron(II) complexes containing 4-substituted-1,2,4-triazole usually display spin crossover properties, which could be used in molecular-based memory devices,<sup>11</sup> displays,<sup>12</sup> and sensors.<sup>13</sup> For instance, the dinuclear iron(II) complex [Fe<sub>2</sub>(**1**)<sub>5</sub>(NCS)<sub>4</sub>]<sub>4</sub>MeOH exhibits both temperature-dependent spin crossover and fluorescence properties.<sup>5d</sup> Furthermore, this complex affords a platform for photomagnetic studies, including the light-induced excited-spin-state trapping (LIESST) and ligand-driven light-induced spin change (LD-LISC) effects,<sup>14</sup> the latter being potentially accessible through the formation of the *trans*-keto form of **1**. **1** is also interesting in its deprotonated form, being able to afford Schiff base mononuclear<sup>15</sup> and polynuclear complexes.<sup>16</sup>

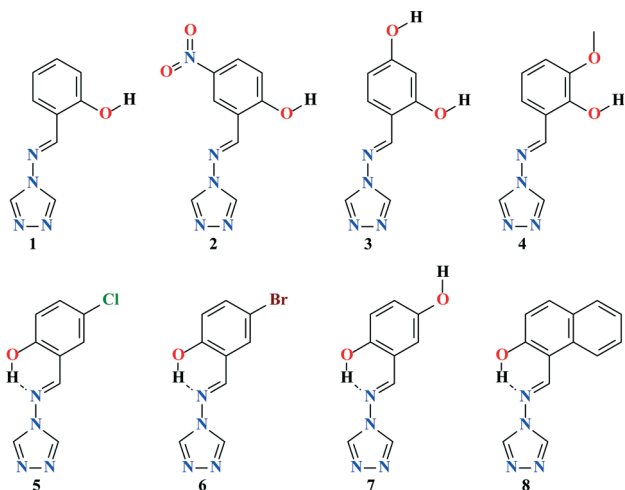


Chart 1

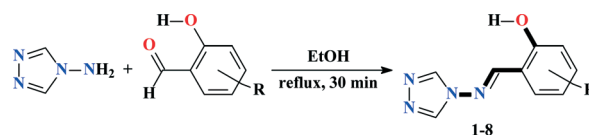
Although both the crystal structure and optical properties of **1** were described recently,<sup>7a</sup> it is also discussed herein for a better comparison within the whole family of the closely related compounds. To examine and discuss the contribution and influence of intermolecular interactions responsible for the crystal packing, Hirshfeld surface analysis<sup>17</sup> and associated 2D fingerprint plots,<sup>18</sup> obtained using the CrystalExplorer 3.1 software,<sup>19</sup> as well as the enrichment ratios,<sup>20</sup> derived as the decomposition of the crystal contact surface between pairs of interacting chemical species, have been performed for the listed compounds. It should be noted that this contribution is only the second one which reports the study of noncovalent interactions by means of Hirshfeld surface analysis in the structures of *N*-salicylidene aniline derivatives.<sup>10t</sup>

## Results and discussion

The *N*-salicylidene-4-amino-1,2,4-triazole-based molecules **1–8** were synthesized by reacting 4-amino-4*H*-1,2,4-triazole with the corresponding salicylaldehyde in ethanol (Scheme 2). The as-synthesized compounds form thin needle-like crystals, which are soluble in most polar solvents and are insoluble in *n*-hexane and diethyl ether. The obtained compounds were divided into two groups, shown in the top and bottom rows in Chart 1, based on the orientation of the *o*-OH group of the *N*-salicylidene fragment as found in their crystal structures (see X-ray description section below).

The <sup>1</sup>H NMR spectra of **1–8** in DMSO-*d*<sub>6</sub> each reveal a single set of signals, which testifies to the presence of a single structure in solution. The signals for the benzene (in **1–7**) and naphthalene (in **8**) protons were found at 6.36–8.84 ppm, while two singlet signals for the arylCHN and triazole protons were observed at 8.97–9.65 and 9.07–9.29 ppm, respectively. The signal of the *o*-OH protons in the spectra of the compounds was shown at 9.77–11.36 ppm. In addition, the spectrum of **7** contains a singlet signal for the second OH proton at 9.13 ppm, while the protons of the two OH fragments in the spectrum of **3** were shown as one singlet at 10.36 ppm. The methoxy protons in the spectrum of **4** were observed as a singlet at 3.85 ppm.

The crystal structures of **1–8** were elucidated by single-crystal X-ray diffraction. Compounds **1–3**, **5**, **6** and **8** crystallize in the monoclinic space groups *P*<sub>2</sub><sub>1</sub>/*n*, *P**c*, *P*<sub>2</sub><sub>1</sub>/*c* and *P*<sub>2</sub><sub>1</sub>, respectively, while the structures of compounds **4** and **7** were refined in the tetragonal space group *P*<sub>4</sub><sub>2</sub>/*n* and trigonal space group *P*<sub>3</sub><sub>1</sub>, respectively. Compounds **1** and **7** contain two and three independent molecules, respectively, in the asymmetric unit, namely **1-I**, **1-II**, **7-I**, **7-II** and **7-III**.



Scheme 2

Molecules in all the structures were found in the enolimine form (Fig. 1–5). The bond lengths of C–O, with respect to the moieties marked in bold in Scheme 2, are about 1.35 Å and those of C–C are about 1.45 Å (Tables 1 and S1 in the ESI†), which indicates single bonds, whereas a double bond of about 1.28 Å is revealed for C–N (Tables 1 and S1 in the ESI†). The bond angles C–C–N and N–N–C of 119.6(2)–

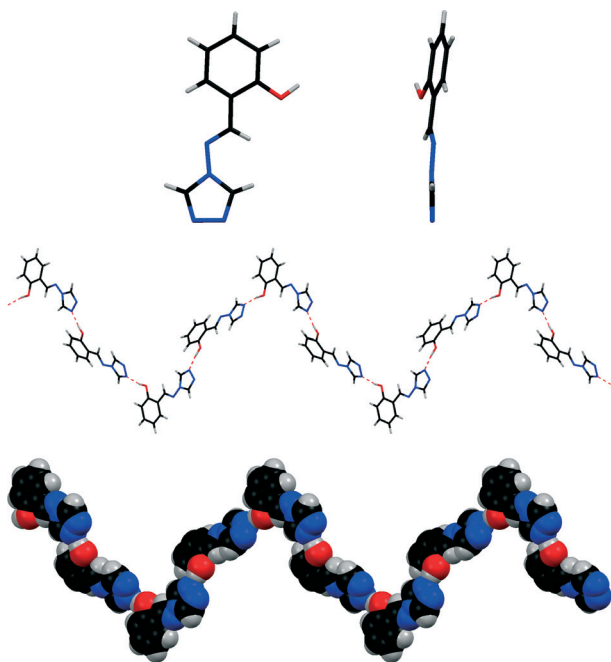


Fig. 1 Top and side views of the molecule structure of 1-I (top), and stick (middle) and spacefill (bottom) hydrogen bonded 1D zigzag chain of molecules in the structure of 1. Colour code: H = grey, C = black, N = blue, O = red.

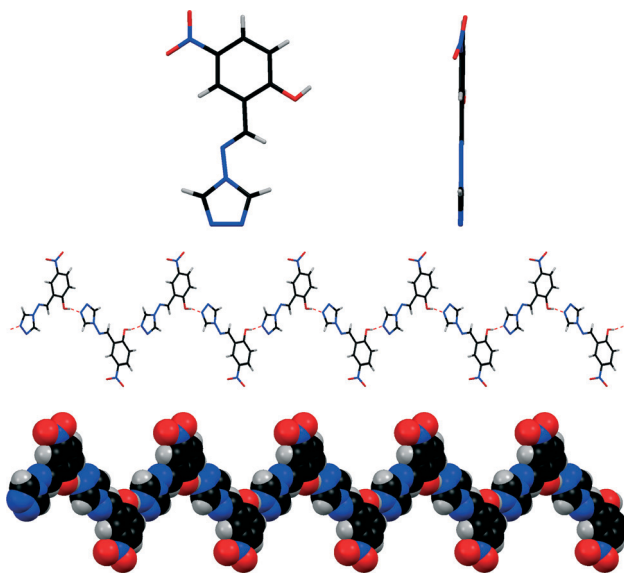


Fig. 2 Top and side views of the molecule structure of 2 (top), and stick (middle) and spacefill (bottom) hydrogen bonded 1D zigzag chain of molecules in the structure of 2. Colour code: H = grey, C = black, N = blue, O = red.

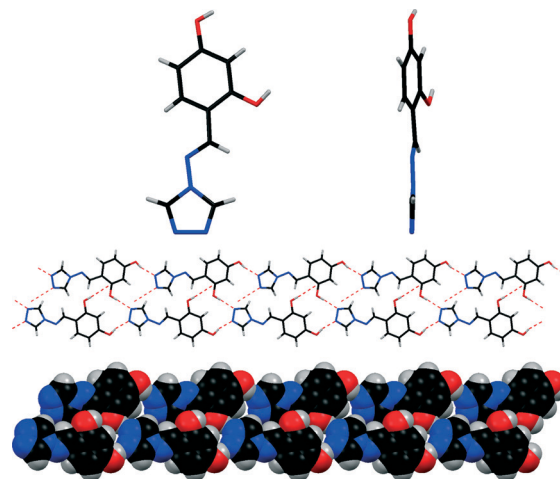


Fig. 3 Top and side views of the molecule structure of 3 (top), and stick (middle) and spacefill (bottom) hydrogen bonded 1D chain of molecules in the structure of 3. Colour code: H = grey, C = black, N = blue, O = red.

122.1(9)° and 115.60(12)–119.4(17)°, respectively, indicate the  $sp^2$ -hybridization of both the carbon and the nitrogen atoms of the imine fragment, further supporting the enolimine form (Tables 1 and S1 in the ESI†). The crucial difference between the structures 1–8 consists of the dihedral angle  $\phi$  between phenol and triazole rings. While in 2 the two rings are at 0.2°, the dihedral angle is larger in 1-II (6.1°), 7-II (6.6°), 7-III (2.0°) and 8 (9.9°) and is significantly larger in 1-I (16.4°), 3 (19.2°), 4 (15.1°), 5 (16.1°), 6 (29.4°) and 7-I (13.5°). Notably, a remarkable change in the dihedral angle between the aromatic rings is also distinguished for the independent

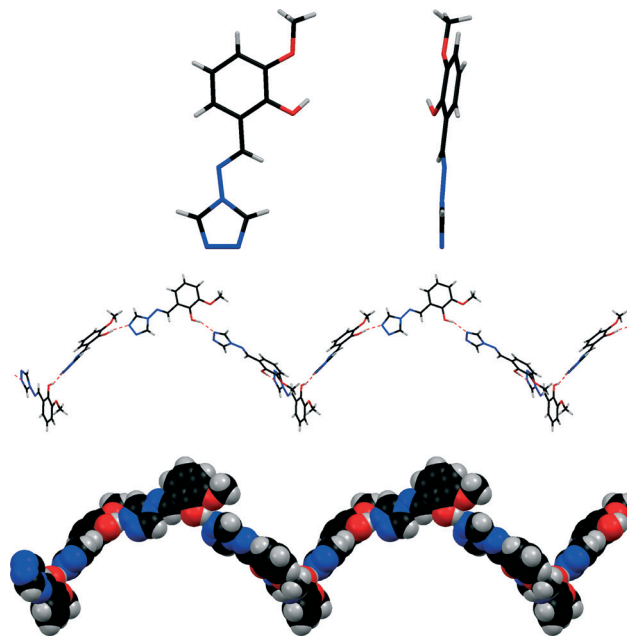


Fig. 4 Top and side views of the molecule structure of 4 (top), and stick (middle) and spacefill (bottom) hydrogen bonded 1D zigzag chain of molecules in the structure of 4. Colour code: H = grey, C = black, N = blue, O = red.

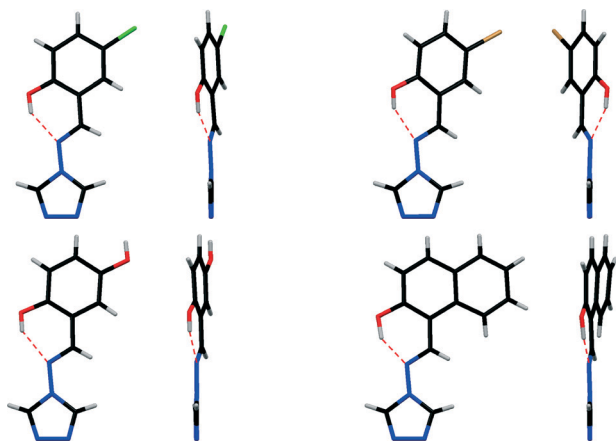


Fig. 5 Top and side views of the molecular structure of **5** (top left), **6** (top right), **7** (bottom left) and **8** (bottom right). Colour code: H = grey, C = black, N = blue, O = red.

molecules in the structures of **1** and **7** (Tables 1 and S1 in the ESI<sup>†</sup>). Both independent molecules in the crystal structure of **1** each develop a new type of molecular geometry where the intramolecular hydrogen bond between the hydroxyl hydrogen atom and the imine nitrogen atom is broken by rotation of the phenolic ring (Chart 1 and Fig. 1) and replaced by a number of intermolecular interactions.<sup>7a</sup> In particular, the formation of an intermolecular hydrogen bond between a nitrogen atom of the triazole ring and the phenolic hydroxyl function is observed (Fig. 1 and Table S2 in the ESI<sup>†</sup>). As a result, a 1D supramolecular zigzag chain is formed (Fig. 1).

In the frame of this work, we also report three more structures **2–4** with the same type of molecular geometry (Chart 1) as well as with the same type of intermolecular hydrogen bond (Fig. 2–4 and Table S2 in the ESI<sup>†</sup>). Furthermore, while molecules in the structures of both **2** and **4** also form a 1D supramolecular zigzag chain (Fig. 2 and 4), the second *p*-OH function in the crystal structure of **3** is also involved in the intermolecular hydrogen bond with the triazole nitrogen atom of the third neighbouring molecule (Fig. 3 and Table S2 in the ESI<sup>†</sup>). As a result, an interlocked double layered 2D sheet is formed (Fig. 3). Notably, the underlying net of **3**, as

analysed by the program TOPOS,<sup>21</sup> has been determined considering molecules as nodes connected through intermolecular hydrogen bonds. The resulting topology is a 4-connected uninodal network with a point Schläfli symbol of {4<sup>4</sup>.6<sup>2</sup>}. This network is identified by an sql/Shubnikov tetragonal plane net topological type in the RCSR database.

Thus, the presence of the triazole ring in the structure of *N*-salicylidene aniline derivatives is crucial and indeed plays a strong structure-directing role, through efficient intermolecular hydrogen bonds, that drives molecules to leave their typical molecular geometry.

The presence of the 1,2,4-triazole ring is of great importance but not enough to break the normal molecular geometry of *N*-salicylidene aniline derivatives. Crystal packing influence has also to be considered. This was clearly defined from the crystal structures of **5–8**, all molecules of which are stabilized by the typical intramolecular hydrogen bond between the hydroxyl hydrogen atom and the imine nitrogen atom (Fig. 5 and Table S2 in the ESI<sup>†</sup>). Notably, the second *m*-OH function in the crystal structure of **7** is involved in the intermolecular hydrogen bond with the triazole nitrogen atom (Fig. 5 and Table S2 in the ESI<sup>†</sup>) similar to those in the structures of **1–4** (Fig. 1–4). However, as a result a 1D supramolecular linear instead of a zigzag chain is formed.

In order to examine the interactions in the crystal structures of **1–8**, the Hirshfeld surface analysis<sup>17</sup> and associated 2D fingerprint plots<sup>18</sup> were obtained using CrystalExplorer 3.1.<sup>19</sup>

Unlike other molecular volumes and surfaces (*e.g.* van der Waals volumes, solvent-accessible surfaces, solvent-excluded surfaces), Hirshfeld surfaces are not simply a function of the molecular geometry but are only defined within the crystal. Consequently, Hirshfeld surfaces reflect the interplay between different atomic sizes and intermolecular contacts in the crystal (condensed phase). Hirshfeld surfaces and volumes are much larger than conventional ones, generally filling at least 95% of the crystal volume,<sup>22</sup> compared with more conventional packing coefficients of between 0.65 and 0.80.<sup>23</sup> Hirshfeld surfaces obviously pack very tightly in the crystal, at most touching and never overlapping. However, quite

Table 1 Selected bond lengths (Å) and angles (°) for **1-I**, **2–6**, **7-I** and **8**<sup>a</sup>

	<b>1-I</b> <sup>b</sup>	<b>2</b>	<b>3</b>	<b>4</b>	<b>5</b>	<b>6</b>	<b>7-I</b> <sup>c</sup>	<b>8</b>
Bond lengths								
C–N	1.279(2)	1.272(4)	1.281(15)	1.270(3)	1.30(2)	1.284(9)	1.313(16)	1.287(5)
C–C	1.458(2)	1.454(5)	1.468(16)	1.464(4)	1.42(2)	1.460(9)	1.436(19)	1.445(5)
C–O	1.3510(19)	1.336(4)	1.370(12)	1.343(3)	1.340(16)	1.363(9)	1.360(17)	1.361(5)
N–N	1.4000(19)	1.398(4)	1.394(13)	1.404(3)	1.38(2)	1.403(8)	1.421(14)	1.394(5)
Bond angles								
C–C–N	121.00(13)	120.8(3)	121.1(10)	119.6(2)	120.5(17)	121.5(6)	120.8(10)	121.7(3)
N–N–C	115.60(12)	117.0(3)	117.4(9)	116.7(2)	119.4(17)	115.8(5)	116.6(9)	117.7(3)
Torsion angles								
C–C–N–N	–175.52(14)	–179.5(3)	177.4(9)	–176.9(2)	177.4(15)	–178.2(6)	177.5(9)	179.3(3)
Dihedral angles (φ)								
Phenol–triazole	16.4	0.2	19.2	15.1	16.1	29.4	13.5	9.9

<sup>a</sup> Values with respect to the moieties marked in bold in Scheme 2. <sup>b</sup> Data for **1-II** are similar to those of **1-I** and are given in the ESI. <sup>c</sup> Data for **7-II** and **7-III** are similar to those of **7-I** and are given in the ESI.

unlike any other partitioning or packing scheme, they leave small intermolecular voids, which can be regarded as regions where the crystalline electron density is very low and is not dominated by any single molecule. The use of Hirshfeld surfaces for the analysis of molecular crystal structures encourages the adoption of a whole structure view of intermolecular interactions, rather than concentrating exclusively on assumed interactions. While the discussion of crystal structures in terms of individual interatom contacts is unavoidable and certainly valuable, a broader picture of intermolecular interactions in the crystal is increasingly desirable; such a picture is available from the Hirshfeld surface. The size and shape of the Hirshfeld surface are intimately related to the chemical environment surrounding the molecule, making it ideal for use in comparing different crystal structures incorporating the same molecule.

The 2D fingerprint plots not only clearly identify each type of intermolecular contact but also enable the analysis of very small differences in these patterns and as such represent an entirely new way of summarizing the major intermolecular contacts of an entire crystal structure in a single 2D colour picture. Fingerprint plots have been shown to be particularly suited to comparing the crystal structures of closely related molecules (*e.g.* polymorphs, different co-crystals, structures with  $Z' > 1.0$ ).

According to the Hirshfeld surface analysis, for both independent molecules of **1** the intermolecular H $\cdots$ H contacts, comprising 30.1% and 34.7% of the total number of contacts, are major contributors to the crystal packing (Tables 2 and S3 in the ESI $^\dagger$ ). The shortest H $\cdots$ H contacts are shown in the fingerprint plots of **1-I** and **1-II** as characteristic broad spikes at  $d_e + d_i \approx 2.2$  Å (Fig. 6 and S1 in the ESI $^\dagger$ ). Furthermore, a subtle feature is evident in the fingerprint plot of **1-I**. There is a splitting of the short H $\cdots$ H fingerprint. This splitting occurs when the shortest contact is between three atoms, rather

than for a direct two-atom contact.<sup>17</sup> The structure of **1-I** is also dominated by H $\cdots$ C and H $\cdots$ N contacts, comprising 21.9% and 34.8%, respectively, while the same contacts in the structure of **1-II** are remarkably less and occupy 17.9% and 25.1%, respectively, of the total Hirshfeld surface areas (Tables 2 and S3 in the ESI $^\dagger$ ).

The H $\cdots$ C contacts in fingerprint plots are shown in the form of “wings” (Fig. 6 and Fig. S1 in the ESI $^\dagger$ ), with the shortest  $d_e + d_i \approx 2.6$ – $2.8$  Å. These contacts are recognized as characteristic of C–H $\cdots$  $\pi$  nature.<sup>17</sup> It is worth adding that the fingerprint plot of **1-I** exhibits a significant number of points at large  $d_e$  and  $d_i$ , shown as tails at the top right of the plot

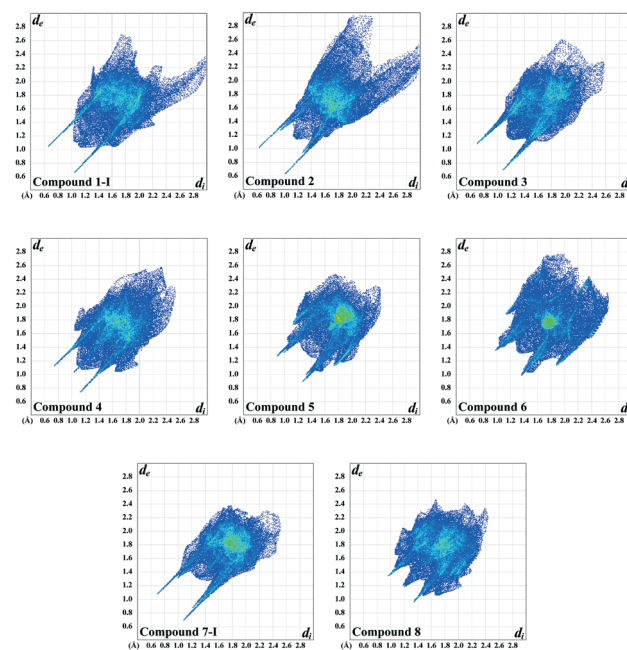


Fig. 6 2D fingerprint plots of observed contacts for **1-I**, **2**–**6**, **7-I** and **8**.

Table 2 Hirshfeld contact surfaces and derived “random contacts” and “enrichment ratios” for **1-I**, **2**, **3** and **4**<sup>a</sup>

	<b>1-I</b>				<b>2</b>				<b>3</b>				<b>4</b>					
	H	C	N	O	H	C	N	O	H	C	N	O	H	C	N	O		
Contacts ( <i>C</i> , %) <sup>b</sup>																		
H	30.1	—	—	—	13.7	—	—	—	29.6	—	—	—	39.4	—	—	—	—	
C	21.9	2.4	—	—	21.5	0.3	—	—	11.3	5.2	—	—	15.7	2.2	—	—	—	
N	34.8	3.5	1.1	—	20.1	5.4	2.4	—	24.2	10.1	0.6	—	24.3	4.5	0.5	—	—	
O	1.2	2.7	1.2	0.0	21.2	3.8	9.3	2.0	16.8	1.6	0.5	0.1	4.6	5.3	3.4	0.1	—	
Surface ( <i>S</i> , %)																		
H	59.1	16.5	20.9	2.6	45.1	15.7	19.8	19.2	55.8	16.7	18.0	9.6	61.7	15.0	16.6	6.8	—	
Random contacts ( <i>R</i> , %)																		
H	34.9	—	—	—	20.3	—	—	—	31.1	—	—	—	38.1	—	—	—	—	
C	19.5	2.7	—	—	14.2	2.5	—	—	18.6	2.8	—	—	18.5	2.3	—	—	—	
N	24.7	1.1	4.4	—	17.9	1.0	3.9	—	20.1	1.0	3.2	—	20.5	0.7	2.8	—	—	
O	3.1	0.9	1.1	0.1	17.3	6.0	7.6	3.7	10.7	3.2	3.5	0.9	8.4	2.0	2.3	0.5	—	
Enrichment ( <i>E</i> ) <sup>c</sup>																		
H	0.86	—	—	—	0.67	—	—	—	0.95	—	—	—	1.03	—	—	—	—	
C	1.12	0.89	—	—	1.51	0.12	—	—	0.61	1.86	—	—	0.85	0.96	—	—	—	
N	1.41	3.18	0.25	—	1.12	5.40	0.62	—	1.20	10.10	0.19	—	1.19	—	0.18	—	—	
O	0.39	3.00	1.09	—	1.23	0.63	1.22	0.54	1.57	0.50	0.14	0.11	0.55	2.65	1.48	—	—	

<sup>a</sup> Data for **1-II** are similar to those of **1-I** and are given in the ESI. <sup>b</sup> Values are obtained from CrystalExplorer 3.1.<sup>19</sup> <sup>c</sup> The enrichment ratios were not computed when the “random contacts” were lower than 0.9%, as they are not meaningful.<sup>20</sup>

(Fig. 6 and S1 in the ESI†). These points, similar to those observed in the fingerprint plot of benzene<sup>17</sup> and phenyl-containing compounds,<sup>24</sup> correspond to regions on the Hirshfeld surface without any close contacts to nuclei in adjacent molecules. The H⋯N contacts in the fingerprint plots of both independent molecules are shown as a pair of sharp spikes at  $d_e + d_i \approx 1.7\text{--}1.8$  Å (Fig. 6 and S1 in the ESI†). These contacts correspond to the N–H⋯O hydrogen bonds (Fig. 1 and Table S1 in the ESI†). The fourth main contribution to intermolecular interactions in the structure of **1-II** arises from H⋯O contacts, comprising 7.4% of the total Hirshfeld surface area (Table S3 in the ESI†) and are shown in the fingerprint plot as a pair of spikes at  $d_e + d_i \approx 2.4$  Å (Fig. S1 in the ESI†). The same contacts in the structure of **1-I** are very negligible and only 1.2% (Tables 2 and S3 in the ESI†). The structures of both molecules of **1** are also described by C⋯C and C⋯N contacts. However, these contacts comprise a negligible proportion of the total Hirshfeld surface area and of 2.4% and 3.5% for **1-I**, and 4.3% and 6.4% for **1-II**, respectively. Moreover, these contacts are shown on the fingerprint plots as the area on the diagonal at  $d_e = d_i \approx 1.7\text{--}2.0$  Å (Fig. 6 and S1 in the ESI†). These contacts are evidence for  $\pi\cdots\pi$  stacking interactions. Close inspection of other intermolecular contacts in the structures of **1-I** and **1-II** also revealed a proportion of C⋯O (1.7–2.7%), N⋯N (1.1–1.7%) and N⋯O (0.7–1.2%) contacts (Tables 2 and S3 in the ESI†).

We have also determined the enrichment ratios ( $E$ )<sup>20</sup> of the intermolecular contacts for both independent molecules of **1** to study the propensity of two chemical species to be in contact. The enrichment ratio, derived from the Hirshfeld surface analysis, is defined as the ratio between the proportion of actual contacts in the crystal and the theoretical proportion of random contacts.  $E$  is larger than unity for a pair of elements with a higher propensity to form contacts, while pairs which tend to avoid contacts yield an  $E$  value lower than unity.

The H⋯H contacts are favoured in the structure of **1-II** since the enrichment ratio  $E_{\text{HH}}$  is close to unity (0.97) and generate a majority (34.7%) of the interaction surface (Table S3 in the ESI†). Contrarily, the H⋯H contacts are less favoured in the structure of **1-I** ( $E_{\text{HH}} = 0.86$ ). This is explained by a significantly lower proportion (30.1%) of H⋯H contacts of the total Hirshfeld surface area in **1-I**, although its structure contains almost the same amount of random contacts as in the structure of **1-II** (Table S3 in the ESI†). The *vice versa* trend is observed for H⋯C contacts, which show an increased propensity to form ( $E_{\text{HC}} = 1.12$ ) in the structure of **1-I**, and only slightly favoured ( $E_{\text{HC}} = 0.86$ ) in **1-II**. This is due to a higher amount of H⋯C contacts of the total Hirshfeld surface area in **1-I** compared to that in **1-II**, despite both structures being characterised by almost the same values of the  $S_{\text{H}}$  proportion and random contacts  $R_{\text{HC}}$  (Tables 2 and S3 in the ESI†). The  $E_{\text{HO}}$  values are larger than unity (1.41 and 1.18) for both molecules of **1**, indicating that H⋯O contacts have an increased propensity to form, with close random contacts. It should be noted that H⋯N contacts are highly

favoured in the structure of **1-II** since the enrichment ratio  $E_{\text{HN}}$  is higher than unity (1.25), while the same contacts in the structure of **1-I** are significantly impoverished ( $E_{\text{HN}} = 0.39$ ). Remarkably, the structure of **1-I** is further characterized by favoured C⋯N contacts ( $E_{\text{CN}} = 3.18$ ), while the same contacts in the structure of **1-II** are even much more favoured ( $E_{\text{CN}} = 5.82$ ). This is due to a negligible amount of random contacts  $R_{\text{CN}}$  (1.1), despite both molecules being characterised by a small amount of C⋯N contacts of the total Hirshfeld surface area (Tables 2 and S3 in the ESI†). However, while the  $E_{\text{CO}}$  value is equal to unity for the structure of **1-II**, the same contacts are much more favoured in the structure of **1-I** ( $E_{\text{CO}} = 3.00$ ), which is explained by a higher amount of the C⋯O contacts on the molecular surface together with a lower amount of random contacts  $R_{\text{CO}}$  for **1-II** compared to those of **1-I** (Tables 2 and S3 in the ESI†). Interestingly, the C⋯C contacts in the structure of **1-II** are remarkably enriched ( $E_{\text{CC}} = 1.43$ ), which is due to a relatively high value of their proportion of the total Hirshfeld surface area. Although the  $S_{\text{C}}$  value and random contacts proportion  $R_{\text{CC}}$  of the structure of **1-I** are almost the same as those for **1-II**, its structure is characterized by fewer C⋯C contacts ( $E_{\text{CC}} = 0.89$ ). This is explained by a smaller amount of C⋯C contacts on the molecular surface of **1-I** (Table 2). The structure of **1-I** is also enriched by N⋯O contacts ( $E_{\text{NO}} = 1.09$ ), while the same contacts in **1-II** are significantly impoverished. Finally, the structures of both molecules are described by impoverished (0.53 for **1-II**) or very impoverished (0.25 **1-I**) N⋯N contacts, which is due to a significantly higher proportion of random contacts  $R_{\text{NN}}$  compared to a proportion of C⋯C contacts on the molecular surface (Tables 2 and S3 in the ESI†).

By introduction of the NO<sub>2</sub> group into the phenolic fragment of **1**, yielding **2**, the contribution of each contact to the total Hirshfeld surface area is changed considerably. In particular, while the proportion of the H⋯C contacts on the molecular surface of **2** is almost the same as for **1-I**, a proportion of both H⋯H and H⋯N contacts decreased significantly up to 13.7% and 20.1%, respectively, with the simultaneous sudden jump of the amount of H⋯O contacts up to 21.2%, the highest value among all the discussed compounds **1–8** (Tables 2 and S3 in the ESI†). This is not surprising and is obviously explained by a terminal position of the NO<sub>2</sub> group on the periphery of a molecule (Fig. 2). The same trend is observed for the corresponding enrichment ratios. While the enrichment ratios  $E_{\text{HC}}$  and  $E_{\text{HN}}$  are notably higher than unity and similar to those in the structure of **1-I**, the  $E_{\text{HH}}$  value decreased significantly, accompanied by a pronounced increase in the  $E_{\text{HO}}$  value (Tables 2 and S3 in the ESI†), which is higher than unity. This indicates that the H⋯O contacts, despite a highly increased proportion of the random contacts  $R_{\text{HO}}$  (Table 1), are favoured in the structure of **2**. The shortest H⋯H contacts are shown in the fingerprint plot of **2** at  $d_e + d_i \approx 2.3\text{--}2.4$  Å (Fig. 6 and S2 in the ESI†). The H⋯C contacts in the fingerprint plot are shown at  $d_e + d_i > 3.1$  Å and an overwhelming majority of points are at larger  $d_e$  and  $d_i$ , shown as tails at the top right of the plot (Fig. 6 and S2 in

the ESI†), which is a characteristic region on the Hirshfeld surface without any close contacts to nuclei in adjacent molecules.<sup>17,19</sup> The H⋯N contacts in the fingerprint plot of 2 are shown as a pair of sharp spikes at  $d_e + d_i \approx 1.7$  Å (Fig. 6 and S1 in the ESI†), similar to those in the fingerprint plots of 1, corresponding to the N–H⋯O hydrogen bonds (Fig. 2 and Table S1 in the ESI†). Moreover, the H⋯O contacts in the fingerprint plot of 2 are also shown as a pair of sharp spikes at  $d_e + d_i \approx 2.3$  Å (Fig. 6 and S1 in the ESI†). Although the structure of 2 is also described by a relatively small proportion of the C⋯N contacts (5.4%) on the total Hirshfeld surface, they are highly favourable as evidenced from the corresponding enrichment ratio ( $E_{CN} = 5.40$ ). At the same time, the enrichment ratios of C⋯O and C⋯C contacts are impoverished or very impoverished compared to those in the structure of 1 (Tables 2 and S3 in the ESI†). This is due to remarkably higher proportions of the random contacts  $R_{CO}$  and  $R_{CC}$  compared to the corresponding proportions of these contacts on the molecular surface. Other intermolecular contacts in the structure of 2 also revealed highly favoured N⋯O (9.3%), and impoverished N⋯N (2.4%) and O⋯O (2.0%) contacts (Table 2).

Moving from 2 to 3, containing a *p*-OH function in the phenolic fragment, and 4, containing a *m*-OMe group in the phenolic part of a molecule, a significant increase in the proportion of the intermolecular H⋯H contacts, comprising 29.6% and 39.4% of the total number of contacts, is observed (Table 2). The proportion of these contacts in the structure of 4 is the most abundant among all the studied compounds 1–8, which is due to the presence of the methyl fragment (Fig. 4). The shortest H⋯H contacts are shown on the fingerprint plots of 3 and 4 at  $d_e + d_i \approx 2.3$  Å and as a sharp spike at  $d_e + d_i \approx 2.1$  Å, respectively (Fig. 6 and S1 and S4 in the ESI†). Although the H⋯H contacts occupy a remarkably higher proportion of the molecular surface as well as produce a higher  $S_H$  value in the structure of 4 compared to those of 3, both compounds are characterised by almost the same enrichment ratio  $E_{HH}$  very close to unity (Table 2). This is caused by a proportional increase of the random contacts  $R_{HH}$  in the structure of 4. Furthermore, the H⋯N contacts in the structure of both 3 and 4 are favoured, occupying the same amount of the total Hirshfeld surface (~24%), and in the fingerprint plot of both compounds are shown as a pair of sharp spikes at  $d_e + d_i \approx 1.8$  Å (Fig. 6 and S3 and S4 in the ESI†), corresponding to the N–H⋯O hydrogen bonds (Fig. 3 and 4 and Table S1 in the ESI†). Both structures are further dominated by H⋯C contacts, comprising 11.3% and 15.7%, respectively, while the random contacts  $R_{HC}$  are the same. All this explains a notable difference in the enrichment ratios  $E_{HC}$  between 3 and 4. This value is 0.85 for 4, characteristic for the less favourable contacts, and 0.61 for 3, indicating an impoverished enrichment. Furthermore, the H⋯C contacts in the fingerprint plot of 4 are shown in the form of clearly pronounced “wings” (Fig. 6 and S4 in the ESI†), with the shortest  $d_e + d_i \approx 2.7$  Å and being characteristic of a C–H⋯ $\pi$  nature.<sup>15</sup> The H⋯O contacts in the structure of 3 also occupy a significant proportion of the molecular surface and

on the corresponding fingerprint plot are shown as a pair of sharp spikes at  $d_e + d_i \approx 2.5$  Å (Fig. 6 and S3 in the ESI†), while the same contacts are negligible in the structure of 4 (Table 1). This is also reflected in the corresponding enrichment ratio  $E_{HO}$ , which is 1.57 for 3 and 0.55 for 4. Thus, the former structure is highly enriched by the H⋯O contacts, while this type of intermolecular contacts is impoverished in the latter structure. The structures of both 3 and 4 are also described by C⋯C and C⋯N contacts. However, these contacts comprise a negligible proportion of the total Hirshfeld surface area in the structure of 4, but remarkably higher in the structure of 3 (Table 2). These contacts are shown on the fingerprint plots as the characteristic area on the diagonal at  $d_e = d_i \approx 1.7$ – $2.0$  Å (Fig. 6 and S3 and S4 in the ESI†) and correspond to  $\pi$ ⋯ $\pi$  stacking interactions. Notably, while the C⋯C contacts are favourable in the structure of 4, as evidenced from the corresponding enrichment ratio  $E_{CC}$  being close to unity, the structure of 3 is more enriched by the same contacts as well as characterised by an extremely enriched value,  $E_{CN} = 10.10$  (Table 2). Two more significant differences in the total Hirshfeld surface areas of 3 and 4 are concealed in the C⋯O and N⋯O intermolecular contacts. These contacts are very negligible in the structure of 3 (1.6% and 0.5%, respectively), while their proportion is remarkably higher in the structure of 4 (5.3% and 3.4%, respectively). All this, together with a higher proportion of the corresponding random contacts  $R_{CO}$  and  $R_{NO}$  in the structure of 3 compared to those of 4, explains the extremely high and poor enrichment ratios of these contacts on their molecular surfaces (Table 2).

The second group of studied compounds (4–8) is characterized by the blocked *o*-OH group of the phenolic fragment due to the formation of the intramolecular hydrogen bond with the imine nitrogen atom (Chart 1 and Fig. 5).

The distribution of main intermolecular contacts, *viz.* H⋯H (19.2% and 17.5%), H⋯N (24.9% and 22.5%), H⋯O (8.8% and 7.3%), C⋯C (9.0% and 7.6%) and H⋯Cl/Br (20.1% and 21.9%), on the total Hirshfeld surface of both 5 and 6 is similar and only minor differences are observed (Table 3). Furthermore, enrichment ratios, corresponding to the listed contacts, are also very similar for both structures. In particular, H⋯N (1.44 and 1.48), H⋯O (1.73 and 1.43) and H⋯Cl/Br (1.73 and 1.62) contacts are highly favoured, and C⋯C (3.21 and 2.92) contacts are even much more favoured. The C⋯C contacts are shown on the fingerprint plots of 5 and 6 as the characteristic pale blue/green area, mixed with yellow and red points, on the diagonal at  $d_e = d_i \approx 1.7$ – $2.0$  Å (Fig. 6 and S5 and S6 in the ESI†), and correspond to the formation of strong  $\pi$ ⋯ $\pi$  stacking interactions. The H⋯N and H⋯O contacts each are shown on the fingerprint plots of 5 and 6 as a pair of sharp spikes at  $d_e + d_i \approx 2.2$ – $2.3$  Å and  $d_e + d_i \approx 2.3$ – $2.5$  Å, respectively (Fig. 6 and S5 and S6 in the ESI†). Interestingly, the H⋯Cl/Br contacts are shown on the fingerprint plots of 5 and 6 as two broad spikes containing pale blue/green points, with the shortest  $d_e + d_i \approx 2.9$  and  $3.0$  Å, respectively (Fig. 6 and S5 and S6 in the ESI†).

**Table 3** Hirshfeld contact surfaces and derived “random contacts” and “enrichment ratios” for **5**, **6**, **7-I** and **8**<sup>a</sup>

	<b>5</b>					<b>6</b>					<b>7-I</b>				<b>8</b>				
	H	C	N	O	Cl	H	C	N	O	Br	H	C	N	O	H	C	N	O	
Contacts ( <i>C</i> , %) <sup>b</sup>																			
H	19.2	—	—	—	—	17.5	—	—	—	—	27.0	—	—	—	29.6	—	—	—	
C	6.4	9.0	—	—	—	11.7	7.6	—	—	—	14.1	5.2	—	—	27.6	3.7	—	—	
N	24.9	6.5	1.3	—	—	22.5	2.9	2.1	—	—	23.7	8.1	0.9	—	22.6	6.7	0.4	—	
O	8.8	0.9	0.0	0.0	—	7.3	2.3	0.0	0.3	—	18.8	0.7	1.0	0.5	9.2	0.1	0.1	0.0	
Cl/Br	20.1	1.7	0.0	0.6	0.6	21.9	0.3	2.1	0.1	1.5	—	—	—	—	—	—	—	—	
Surface ( <i>S</i> , %)	49.3	16.8	17.0	5.2	11.8	49.2	16.2	15.9	5.2	13.7	55.3	16.7	17.3	10.8	59.3	20.9	15.1	4.7	
Random contacts ( <i>R</i> , %)																			
H	24.3	—	—	—	—	24.2	—	—	—	—	30.6	—	—	—	35.2	—	—	—	
C	16.6	2.8	—	—	—	15.9	2.6	—	—	—	18.5	2.8	—	—	24.8	4.4	—	—	
N	16.8	5.7	2.9	—	—	15.6	5.2	2.5	—	—	19.1	1.0	3.0	—	17.9	1.3	2.3	—	
O	5.1	1.7	1.8	0.3	—	5.1	1.7	1.7	0.3	—	11.9	3.6	3.7	1.2	5.6	2.0	1.4	0.2	
Cl/Br	11.6	4.0	4.0	1.2	1.4	13.5	4.4	4.3	1.4	1.9	—	—	—	—	—	—	—	—	
Enrichment ( <i>E</i> ) <sup>c</sup>																			
H	0.79	—	—	—	—	0.72	—	—	—	—	0.88	—	—	—	0.84	—	—	—	
C	0.39	3.21	—	—	—	0.74	2.92	—	—	—	0.76	1.86	—	—	1.11	0.84	—	—	
N	1.48	1.14	0.45	—	—	1.44	0.56	0.84	—	—	1.24	8.10	0.30	—	1.26	5.15	0.17	—	
O	1.73	0.53	0.00	—	—	1.43	1.35	0.00	—	—	1.58	0.19	0.27	0.42	1.64	0.05	0.07	—	
Cl/Br	1.73	0.43	0.00	0.50	0.43	1.62	0.07	0.49	0.07	0.79	—	—	—	—	—	—	—	—	

<sup>a</sup> Data for **7-II** and **7-III** are similar to those of **7-I** and are given in the ESI. <sup>b</sup> Values are obtained from CrystalExplorer 3.1.<sup>19</sup> <sup>c</sup> The enrichment ratios were not computed when the “random contacts” were lower than 0.9%, as they are not meaningful.<sup>20</sup>

The H···H contacts in both structures are less favoured ( $E_{HH} = 0.79$  and  $0.72$ , respectively), which is due to relatively higher values of the random contacts  $R_{HH}$  compared to the proportion of these contacts on the molecular surface.

The H···C intermolecular contacts occupy 6.4% of the molecular surface in the structure of **5**, while the same contacts are about two times more in the structure of **6** (Table 3). However, the proportion of the random contacts  $R_{HC}$  is similar (~16%) and relatively high for both structures, yielding less favourable for enrichment ratios **6** and impoverished for **5** (Table 2). The H···C contacts in the fingerprint plots of **5** and **6** are shown as diffusely spread points (Fig. 6 and S5 and S6 in the ESI†), with the shortest  $d_e + d_i \approx 3.2$  Å. The *vice versa* trend is observed for C···N contacts, which show an increased propensity to form ( $E_{CN} = 1.14$ ) in the structure of **5**, and impoverished ( $E_{CN} = 0.56$ ) in **6**. This is due to about two times higher amount of C···N contacts of the total Hirshfeld surface area in **5** compared to that in **6**, despite both structures being characterised by almost the same values of  $S_C$  and  $S_N$  as well as random contacts  $R_{CN}$  (Table 3). Contrarily to the C···N contacts, the structure of **5** contains a negligible amount of the C···O contacts (0.9%), while the proportion of the same contacts is two and a half times more (2.3%) on the total Hirshfeld surface area of **6**. All this, together with the same value of the random contacts  $R_{CO}$  for both structures, show that the molecular surface of **6** is highly enriched with the C···O contacts, while they are impoverished on the surface of **5** (Table 3). Some other negligible intermolecular contacts were found in the structures of **5** and **6** (Table 3).

The distribution of intermolecular contacts, as well as their corresponding enrichment ratios, is very similar for all the three independent molecules in the structure of **7** and,

surprisingly, close to values found for the intermolecular contacts on the total Hirshfeld surface of **3** (Tables 2 and S3 in the ESI†). Thus, the position of the second OH group in the phenolic fragment as well as the fact that the *o*-OH group is involved in intermolecular hydrogen bonding in the structure of **3** and that the same function is blocked by the intramolecular hydrogen bonding in the structures of all independent molecules of **7**, almost have no influence on the type, distribution and enrichment ratios of contacts on the molecular surfaces of **3** and **7**. The main difference, however, arises from the distribution of the H···O contacts on the fingerprint plots. These contacts are shown on the fingerprint plots of each independent molecule of **7** as two sharp spikes at much shorter  $d_e + d_i \approx 2.2$  Å compared to that of **3** (Fig. 6 and S3 and S7 in the ESI†).

According to the Hirshfeld surface analysis, for **8** the intermolecular H···H contacts, comprising 29.6% of the total number of contacts, are major contributors to the crystal packing (Table 3). The shortest H···H contacts are shown in the fingerprint plot as a sharp spike at  $d_e + d_i \approx 2.4$  Å (Fig. 6 and S8 in the ESI†). The structure of **8** is also dominated by H···C, H···N and H···O contacts, comprising 27.6%, 22.6% and 9.2%, respectively, of the total Hirshfeld surface areas (Table 2). The former contacts in the fingerprint plot are shown in the form of clearly pronounced “wings” (Fig. 6 and S8 in the ESI†), with the shortest  $d_e + d_i \approx 2.7$  Å, corresponding to C–H··· $\pi$  interactions.<sup>17</sup> The latter two contacts are shown on the fingerprint plot of **8** as two sharp, for H···N, or broad, for H···O, spikes with the shortest  $d_e + d_i \approx 2.3$  and 2.6 Å, respectively (Fig. 6 and S8 in the ESI†). The H···C, H···N and H···O contacts are highly favoured in the structure of **8** since the corresponding enrichment ratios  $E_{HH}$  are

higher than unity (1.11–1.64). Contrarily, the H $\cdots$ H contacts are less favoured ( $E_{\text{HH}} = 0.84$ ) even though they generate a majority of the interaction surface. This is explained by a relatively higher proportion of the random contacts  $R_{\text{HH}}$  (Table 3). The last two moderate contributors into the molecular surface in the structure of **8** are C $\cdots$ C and C $\cdots$ N contacts. Contrary to expectations, based on the presence of the naphthalene fragment, the former contacts occupy only 3.7% of the total Hirshfeld surface, while the proportion of the latter ones is about two times more and of 6.7%. Furthermore, the molecular surface of **8** is highly enriched with the C $\cdots$ N contacts, as evidenced from the corresponding enrichment ratio,  $E_{\text{CN}} = 5.15$ , while the C $\cdots$ C contacts are significantly less favourable ( $E_{\text{CN}} = 0.84$ ). Other intermolecular contacts in the structure of **8** occupy a very negligible proportion of the molecular surface (0.6%) and are very impoverished (Table 3).

Compounds **1–8** were analyzed by diffuse reflectance spectroscopy (DRS) as pure solid powders to avoid matrix and environment effects that are known to intensively modify the optical properties of *N*-salicylidene aniline derivatives.<sup>5b</sup> The diffuse reflectance spectra of **1**, **3** and **4**, for which a Kubelka–Munk (KM) treatment was applied, each exhibit bands exclusively in the UV region (Fig. 7 and Table 4), which is typical of the enol form. In the spectra of **5** and **6** the enol band is slightly shifted to lower energies, which is caused by the presence of *m*-Cl/Br substituents in the phenolic fragment, while in the spectrum of **8** this shift is more remarkable due to the naphthalene fragment (Fig. 7 and Table 4). The presence of the second *m*-OH group in the phenolic fragment of **7** also resulted in the bathochromic shift of the enol band; however, its spectrum is also characterised by a broad shoulder centred at about 500 nm and ranging up to 600 nm (Fig. 7 and Table 4). This band in the visible range of the spectrum is responsible for the orange colour of the crystals of **7** and is typical of the *cis*-keto form of the molecule. A similar low intense shoulder, but up to about 500 nm, is also present in the spectrum of **2** (Fig. 7 and Table 4) and is responsible for the pale yellow colour of its crystals. However, in this case the band in the visible range of the spectrum is mainly due to the presence of the chromophoric nitro group. All the studied compounds **1–8** were observed to be non photochromic regardless of the irradiation wavelength ( $\lambda = 254, 365, 450$  and  $546$  nm) and time, while **7** was found to be thermochromic from coloured to colourless upon cooling with liquid nitrogen (Fig. 7).

Among the structures of **5–8**, which potentially can exhibit chromic properties due to the intramolecular hydrogen N–H $\cdots$ O bond, only **7** exhibits thermochromic properties. This might be explained by the presence of highly favourable C $\cdots$ C and even much more favourable C $\cdots$ N contacts and slightly impoverished H $\cdots$ C contacts together with the absence of highly favourable H $\cdots$ Hal contacts, as in the structures of halogen-containing compounds **5** and **6**, on the molecular surface of **7**, while the opposite trend is observed for **5**, **6** and **8** (Table 3). In other words, the presence of  $\pi\cdots\pi$  intermolecular interactions accompanied by the decreased C–

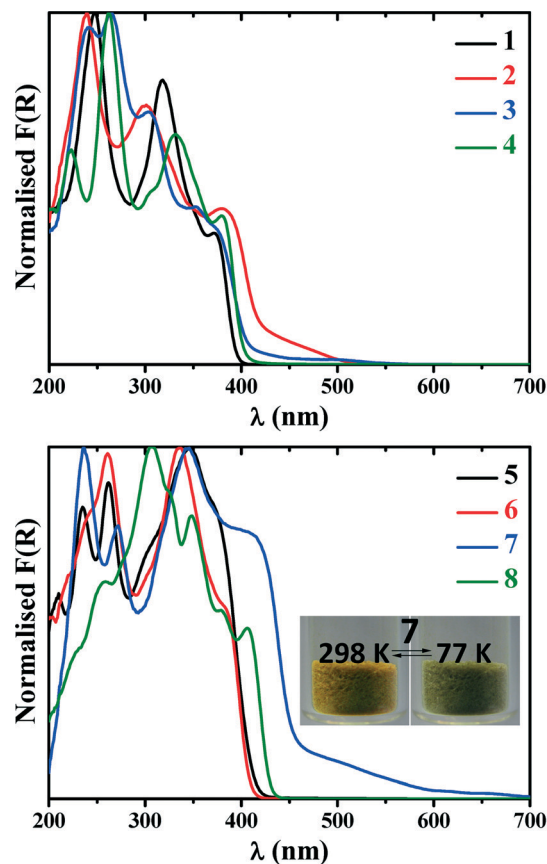


Fig. 7 Normalised KM spectra of **1–8** at 23 °C and photographs showing thermochromism for **7**.

H $\cdots$  $\pi$  interactions are highly favourable to facilitating the generation of the *cis*-keto form. These two situations can also influence the energy differences between ground and excited states, which, in turn, can favour the formation of the *cis*-keto form. However, to check this hypothesis detailed and in-depth theoretical studies are needed.

Regarding the relationship between the intermolecular interactions and the existence of the enol or *cis*-keto forms of **1–8**, one must keep in mind that the Hirshfeld surface analysis can only be run after the crystal structure is obtained from X-ray analysis. Since no crystal structures of the *cis*-keto forms of **1–8** were obtained, such a relationship for the enol and *cis*-keto forms cannot be discussed yet. Notably, if the same form of a molecule results in two or several polymorphs, different Hirshfeld surfaces with different contributions of

Table 4  $\lambda_{\text{max}}$  of the bands in diffuse reflectance spectra of **1–8**

<b>1</b>	248, 318, 372
<b>2</b>	239, 301, 381, 430 (sh.)
<b>3</b>	241, 264, 354 (sh.), 373 (sh.)
<b>4</b>	223, 262, 306 (sh.), 331, 379
<b>5</b>	235, 262, 306 (sh.), 345, 371 (sh.)
<b>6</b>	242 (sh.), 261, 336, 381 (sh.)
<b>7</b>	236, 272, 344, 400 (sh.), 490 (sh., <i>cis</i> -keto)
<b>8</b>	230 (sh.), 257, 307, 325 (sh.), 348, 380 (sh.), 406

certain contacts are obviously produced. This can be complicated if different solvomorphs of the same molecule can be obtained too. Furthermore, since the enol to *cis*-keto transformation is exclusively an intramolecular process, where the Hirshfeld surface analysis is completely blind, it might mean that different forms (enol and *cis*-keto) could generate the same Hirshfeld surface keeping the overall geometry of a molecule.

## Conclusions

In summary, a series of eight closely related *N*-salicylidene-4-amino-1,2,4-triazole compounds 1–8 has successfully been prepared by the condensation reaction of the corresponding aldehyde with 4-amino-4*H*-1,2,4-triazole. All the obtained compounds were studied by means of <sup>1</sup>H NMR spectroscopy in solution, revealing the presence of a single structure at least in DMSO-*d*<sub>6</sub>.

According to single-crystal X-ray diffraction, it was established that the crystal structures of 5–8 each are stabilized by a linear intramolecular hydrogen bond of the O–H⋯N type, formed between the *o*-OH hydrogen atom of the phenolic ring and the imine nitrogen atom. The same *o*-OH function in the crystal structures of 1–4 was found to be involved in intermolecular hydrogen bonds with one of the triazole nitrogen atoms of the adjacent molecule. The overall geometry of each molecule in the structures of 1–8 was found to be almost planar or slightly deviated from planarity.

Hirshfeld surface analysis showed that the structures of all compounds are mainly characterized by H⋯H, H⋯C, H⋯N and H⋯O contacts as well as some contribution from C⋯C and C⋯N contacts is clearly observed.

Diffuse reflectance spectroscopy reveals the exclusive presence of the enol form in the solid state at room temperature for 1–6 and 8, while a mixture of dominant enol and *cis*-keto forms was found for 7. All the studied compounds 1–8 were observed to be non photochromic, while 7 was found to be thermochromic from coloured to colourless upon cooling.

This work, being an attempt to study noncovalent interactions in a series of structures of *N*-salicylidene aniline derivatives by means of Hirshfeld surface analysis, might stimulate further crystal engineering of the described compounds.

## Experimental

### Physical measurements

<sup>1</sup>H NMR spectra in DMSO-*d*<sub>6</sub> were obtained on a Bruker AC 300 MHz spectrometer at 25 °C. Diffuse reflectance spectra were obtained with a Varian Cary 5E spectrometer using polytetrafluoroethylene (PTFE) as a reference. Spectra were measured on pure solids to avoid matrix effects. Eventual distortions in the Kubelka–Munk spectra that could result from the study of pure compounds have not been considered because no comparison with absorption spectra was necessary. Light irradiations were carried out with a LOT-ORIEL 200 W high-

pressure mercury arc lamp (LSN261). Elemental analyses were performed on a CHNS HEKAtech EuroEA 3000 analyzer.

### Hirshfeld surface analysis

The Hirshfeld molecular surfaces<sup>17</sup> and their associated 2D fingerprint plots<sup>18</sup> were generated using the CrystalExplorer 3.1 software<sup>19</sup> on the basis of crystal structures. The *d*<sub>norm</sub> (normalized contact distance) surface and the breakdown of the 2D fingerprint plots were used for decoding and quantifying the intermolecular interactions in the crystal lattice. The *d*<sub>norm</sub> is a symmetric function of distances to the surface from the nuclei inside (*d*<sub>i</sub>) and outside (*d*<sub>e</sub>) the Hirshfeld surface, relative to their respective van der Waals radii. 2D fingerprint plots were generated using *d*<sub>i</sub> and *d*<sub>e</sub> in the translated 0.4–3.0 Å range and including reciprocal contacts as a pair of coordinates in 2D histograms. A colour gradient in the fingerprint plots ranging from blue to red is used to visualize the proportional contribution of contact pairs in the global surface.

### Enrichment ratio

The enrichment ratio (*E*)<sup>20</sup> of a pair of elements (*X*,*Y*) is the ratio between the proportion of actual contacts in the crystal and the theoretical proportion of random contacts. *E* is larger than unity for pairs of elements which have a high propensity to form contacts in crystals, while pairs which tend to avoid contacts with each other yield an *E* value lower than unity. *E* values are calculated from the percentage of contacts, which, in turn, are given by the CrystalExplorer 3.1 software,<sup>19</sup> between one type or two types of chemical elements in a crystal packing.

### Synthesis of 1–8

All compounds were synthesized according to the previously described procedure.<sup>7a</sup> A solution of salicylaldehyde, 5-nitrosalicylaldehyde, β-resorcyaldehyde, *o*-vanillin, 5-chlorosalicylaldehyde, 5-bromosalicylaldehyde, gentisaldehyde or 2-hydroxy-1-naphthaldehyde (10 mmol; 1.221, 1.671, 1.381, 1.522, 1.566, 2.010, 1.381 and 1.722 g, respectively) dissolved in ethanol (20 mL) was added to a solution of 4-amino-4*H*-1,2,4-triazole (10 mmol, 0.841 g) in the same solvent (20 mL). The mixture was stirred for 30 min and, afterwards, heated at reflux for 1 h. The resulting solution was allowed to cool to room temperature to give crystals of 1–8.

1. <sup>1</sup>H NMR: δ = 6.94 (t, d, <sup>3</sup>*J*<sub>H,H</sub> = 7.3 Hz, <sup>4</sup>*J*<sub>H,H</sub> = 0.9 Hz, 1H, *m*-H, C<sub>6</sub>H<sub>4</sub>), 6.99 (d, d, <sup>3</sup>*J*<sub>H,H</sub> = 8.3 Hz, <sup>4</sup>*J*<sub>H,H</sub> = 0.9 Hz, 1H, *m*-H, C<sub>6</sub>H<sub>4</sub>), 7.41 (t, d, <sup>3</sup>*J*<sub>H,H</sub> = 7.3 Hz, <sup>4</sup>*J*<sub>H,H</sub> = 1.7 Hz, 1H, *p*-H, C<sub>6</sub>H<sub>4</sub>), 7.78 (d, d, <sup>3</sup>*J*<sub>H,H</sub> = 7.8 Hz, <sup>4</sup>*J*<sub>H,H</sub> = 1.7 Hz, 1H, *o*-H, C<sub>6</sub>H<sub>4</sub>), 9.15 (s, 1H, arylCHN), 9.17 (s, 2H, triazole), 10.49 (br. s, 1H, OH) ppm. Calc. for C<sub>9</sub>H<sub>8</sub>N<sub>4</sub>O (188.19): C 57.44, H 4.28; N 29.77. Found: C 57.49, H 4.31, N 29.81.

2. <sup>1</sup>H NMR: δ = 7.05 (d, <sup>3</sup>*J*<sub>H,H</sub> = 8.8 Hz, 1H, *m*-H, C<sub>6</sub>H<sub>3</sub>), 7.49 (d, d, <sup>3</sup>*J*<sub>H,H</sub> = 8.8 Hz, <sup>4</sup>*J*<sub>H,H</sub> = 2.6 Hz, 1H, *p*-H, C<sub>6</sub>H<sub>3</sub>), 7.82 (d, <sup>4</sup>*J*<sub>H,H</sub> = 2.6 Hz, 1H, *o*-H, C<sub>6</sub>H<sub>3</sub>), 9.06 (s, 1H, arylCHN), 9.22 (s, 2H, triazole), 10.84 (br. s, 1H, OH) ppm. Calc. for

$C_9H_7N_5O_3$  (233.19): C 46.36, H 3.03; N 30.03. Found: C 46.41, H 2.99, N 30.09.

3.  $^1H$  NMR:  $\delta$  = 6.36–6.43 (m, 2H, *m*-H,  $C_6H_3$ ), 7.60 (d,  $^3J_{H,H}$  = 6.6 Hz, 1H, *o*-H,  $C_6H_3$ ), 8.97 (s, 1H, arylCHN), 9.07 (s, 2H, triazole), 10.36 (br. s, 2H, OH) ppm. Calc. for  $C_9H_8N_4O_2$  (204.19): C 52.94, H 3.95; N 27.44. Found: C 52.98, H 3.91, N 27.48.

4.  $^1H$  NMR:  $\delta$  = 3.85 (s, 3H, MeO), 6.90 (t,  $^3J_{H,H}$  = 8.1 Hz, 1H, *m*-H,  $C_6H_3$ ), 7.15 (d. d,  $^3J_{H,H}$  = 8.1 Hz,  $^4J_{H,H}$  = 1.5 Hz, 1H, *p*-H,  $C_6H_3$ ), 7.38 (d. d,  $^3J_{H,H}$  = 8.1 Hz,  $^4J_{H,H}$  = 1.5 Hz, 1H, *o*-H,  $C_6H_3$ ), 9.17 (s, 3H, arylCHN + triazole), 9.87 (br. s, 1H, OH) ppm. Calc. for  $C_{10}H_{10}N_4O_2$  (218.22): C 55.04, H 4.62; N 25.68. Found: C 55.10, H 4.67, N 25.62.

5.  $^1H$  NMR:  $\delta$  = 7.01 (d,  $^3J_{H,H}$  = 8.8 Hz, 1H, *m*-H,  $C_6H_3$ ), 7.43 (d. d,  $^3J_{H,H}$  = 8.8 Hz,  $^4J_{H,H}$  = 2.6 Hz, 1H, *p*-H,  $C_6H_3$ ), 7.75 (d,  $^4J_{H,H}$  = 2.6 Hz, 1H, *o*-H,  $C_6H_3$ ), 9.09 (s, 1H, arylCHN), 9.18 (s, 2H, triazole), 10.81 (br. s, 1H, OH) ppm. Calc. for  $C_9H_7ClN_4O$  (222.63): C 48.55, H 3.17; N 25.17. Found: C 48.62, H 3.12, N 25.14.

6.  $^1H$  NMR:  $\delta$  = 6.96 (d,  $^3J_{H,H}$  = 8.8 Hz, 1H, *m*-H,  $C_6H_3$ ), 7.54 (d. d,  $^3J_{H,H}$  = 8.8 Hz,  $^4J_{H,H}$  = 2.6 Hz, 1H, *p*-H,  $C_6H_3$ ), 7.89 (d,  $^4J_{H,H}$  = 2.6 Hz, 1H, *o*-H,  $C_6H_3$ ), 9.09 (s, 1H, arylCHN), 9.19 (s, 2H, triazole), 10.81 (s, 1H, OH) ppm. Calc. for  $C_9H_7BrN_4O$  (267.08): C 40.47, H 2.64; N 20.98. Found: C 40.51, H 2.68, N 21.03.

7.  $^1H$  NMR:  $\delta$  = 6.82 (d,  $^3J_{H,H}$  = 8.8 Hz, 1H, *m*-H,  $C_6H_3$ ), 6.87 (d. d,  $^3J_{H,H}$  = 8.8 Hz,  $^4J_{H,H}$  = 2.6 Hz, 1H, *p*-H,  $C_6H_3$ ), 7.18 (d,  $^4J_{H,H}$  = 2.6 Hz, 1H, *o*-H,  $C_6H_3$ ), 9.06 (s, 1H, arylCHN), 9.13 (s, 1H, *m*-OH), 9.15 (s, 2H, triazole), 9.77 (s, 1H, *o*-OH) ppm. Calc. for  $C_9H_8N_4O_2$  (204.19): C 52.94, H 3.95; N 27.44. Found: C 52.87, H 3.99, N 27.50.

8.  $^1H$  NMR:  $\delta$  = 7.27 (d,  $^3J_{H,H}$  = 9.2 Hz, 1H, 3-H,  $C_{10}H_6$ ), 7.43 (t,  $^3J_{H,H}$  = 7.5 Hz, 1H, 6-H,  $C_{10}H_6$ ), 7.61 (t,  $^3J_{H,H}$  = 7.5 Hz, 1H, 7-H,  $C_{10}H_6$ ), 7.90 (d,  $^3J_{H,H}$  = 7.7 Hz, 1H, 5-H,  $C_{10}H_6$ ), 8.04 (d,  $^3J_{H,H}$  = 8.8 Hz, 1H, 4-H,  $C_{10}H_6$ ), 8.84 (d,  $^3J_{H,H}$  = 8.4 Hz, 1H, 8-H,  $C_{10}H_6$ ), 9.29 (s, 2H, triazole), 9.65 (s, 1H, arylCHN), 11.36 (br. s, 1H, OH) ppm. Calc. for  $C_{13}H_{10}N_4O$  (238.25): C 65.54, H 4.23; N 23.52. Found: C 65.62, H 4.29, N 23.46.

### Single-crystal X-ray diffraction study

X-ray data collection from 2–8 was performed on a Mar345 image plate detector using Mo-K $\alpha$  radiation (Rigaku UltraX 18S generator, Xenocs Fox3D mirror). The data were integrated using the CrysAlisPro software.<sup>25</sup> The implemented empirical absorption correction was applied. All structures were solved by direct methods using the SHELXS97 program<sup>26</sup> and refined by full-matrix least squares on  $|F^2|$  using SHELXL2014/7.<sup>27</sup> Non-hydrogen atoms were anisotropically refined and the hydrogen atoms were placed on calculated positions in riding mode with temperature factors fixed at 1.2 times  $U_{eq}$  of the parent atoms and 1.5 times  $U_{eq}$  for the methyl hydrogens. The crystals of 3 and 6 were identified as non-merohedral twins and integrated as such. For 5 the twinrotmat algorithm in Platon<sup>28</sup> was applied to separate three twin domains. Refinement of these three structures was

completed against an HKLF5 formatted reflection file. For all, structure data were recorded up to 0.83 Å. Data cut-offs were, however, made during integration/refinement based on  $I/\sigma$ , and  $R_{int}$  values for the outer resolution shells are 1, 1.04 and 0.95 Å for 3, 5 and 7, respectively. Figures were generated using the program Mercury.<sup>29</sup>

**Crystal data for 1<sup>7a</sup>.**  $C_9H_8N_4O$ ,  $M_r$  = 188.19 g mol<sup>-1</sup>, monoclinic, space group  $P2_1/n$ ,  $a$  = 5.101(2),  $b$  = 28.807(9),  $c$  = 12.029(5) Å,  $\beta$  = 93.20(2)°,  $V$  = 1764.8(11) Å<sup>3</sup>,  $T$  = 120(2) K,  $Z$  = 8,  $\rho$  = 1.417 g cm<sup>-3</sup>,  $\mu$ (Mo-K $\alpha$ ) = 0.099 mm<sup>-1</sup>, reflections: 25 383 collected, 3490 unique,  $R_{int}$  = 0.047,  $R_1$ (all) = 0.0486,  $wR_2$ (all) = 0.1143.

**Crystal data for 2.**  $C_9H_7N_5O_3$ ,  $M_r$  = 233.20 g mol<sup>-1</sup>, monoclinic, space group  $P2_1/n$ ,  $a$  = 5.3288(4),  $b$  = 18.3034(13),  $c$  = 10.3561(8) Å,  $\beta$  = 94.819(7)°,  $V$  = 1006.51(13) Å<sup>3</sup>,  $T$  = 150(2) K,  $Z$  = 4,  $\rho$  = 1.539 g cm<sup>-3</sup>,  $\mu$ (Mo-K $\alpha$ ) = 0.121 mm<sup>-1</sup>, reflections: 6795 collected, 1826 unique,  $R_{int}$  = 0.146,  $R_1$ (all) = 0.1234,  $wR_2$ (all) = 0.1670.

**Crystal data for 3.**  $C_9H_8N_4O_2$ ,  $M_r$  = 204.19 g mol<sup>-1</sup>, monoclinic, space group  $P2_1/n$ ,  $a$  = 5.8474(12),  $b$  = 21.040(4),  $c$  = 7.5567(18) Å,  $\beta$  = 107.25(2)°,  $V$  = 887.9(3) Å<sup>3</sup>,  $T$  = 298(2) K,  $Z$  = 4,  $\rho$  = 1.528 g cm<sup>-3</sup>,  $\mu$ (Mo-K $\alpha$ ) = 0.113 mm<sup>-1</sup>, reflections: 1626 collected, 1626 unique,  $R_{int}$  = 0.000,  $R_1$ (all) = 0.1607,  $wR_2$ (all) = 0.1998.

**Crystal data for 4.**  $C_{10}H_{10}N_4O_2$ ,  $M_r$  = 218.22 g mol<sup>-1</sup>, tetragonal, space group  $P4_2/n$ ,  $a$  = 19.9241(13),  $b$  = 19.9241(13),  $c$  = 5.1153(5) Å,  $V$  = 2030.6(3) Å<sup>3</sup>,  $T$  = 298(2) K,  $Z$  = 8,  $\rho$  = 1.428 g cm<sup>-3</sup>,  $\mu$ (Mo-K $\alpha$ ) = 0.104 mm<sup>-1</sup>, reflections: 11 261 collected, 1798 unique,  $R_{int}$  = 0.106,  $R_1$ (all) = 0.1008,  $wR_2$ (all) = 0.1221.

**Crystal data for 5.**  $C_9H_7ClN_4O$ ,  $M_r$  = 222.64 g mol<sup>-1</sup>, monoclinic, space group  $Pc$ ,  $a$  = 3.7737(14),  $b$  = 14.259(5),  $c$  = 8.993(3) Å,  $\beta$  = 101.23(4)°,  $V$  = 474.6(3) Å<sup>3</sup>,  $T$  = 150(2) K,  $Z$  = 2,  $\rho$  = 1.558 g cm<sup>-3</sup>,  $\mu$ (Mo-K $\alpha$ ) = 0.378 mm<sup>-1</sup>, reflections: 849 collected, 849 unique,  $R_{int}$  = 0.000,  $R_1$ (all) = 0.0831,  $wR_2$ (all) = 0.2008.

**Crystal data for 6.**  $C_9H_7BrN_4O$ ,  $M_r$  = 267.10 g mol<sup>-1</sup>, monoclinic, space group  $P2_1/c$ ,  $a$  = 13.4933(16),  $b$  = 10.4263(13),  $c$  = 7.2548(13) Å,  $\beta$  = 93.731(13)°,  $V$  = 1018.5(3) Å<sup>3</sup>,  $T$  = 180(2) K,  $Z$  = 4,  $\rho$  = 1.742 g cm<sup>-3</sup>,  $\mu$ (Mo-K $\alpha$ ) = 4.013 mm<sup>-1</sup>, reflections: 2757 collected, 2757 unique,  $R_{int}$  = 0.000,  $R_1$ (all) = 0.0704,  $wR_2$ (all) = 0.1573.

**Crystal data for 7.**  $C_9H_8N_4O_2$ ,  $M_r$  = 204.19 g mol<sup>-1</sup>, trigonal, space group  $P3_1$ ,  $a$  = 11.7895(5),  $b$  = 11.7895(5),  $c$  = 17.6053(8) Å,  $\gamma$  = 120°,  $V$  = 2119.2(2) Å<sup>3</sup>,  $T$  = 298(2) K,  $Z$  = 9,  $\rho$  = 1.440 g cm<sup>-3</sup>,  $\mu$ (Mo-K $\alpha$ ) = 0.107 mm<sup>-1</sup>, reflections: 3464 collected, 3464 unique,  $R_{int}$  = 0.000,  $R_1$ (all) = 0.0669,  $wR_2$ (all) = 0.1121.

**Crystal data for 8.**  $C_{13}H_{10}N_4O$ ,  $M_r$  = 238.25 g mol<sup>-1</sup>, monoclinic, space group  $P2_1$ ,  $a$  = 8.7625(6),  $b$  = 5.8854(4),  $c$  = 11.0081(12) Å,  $\beta$  = 91.833(7)°,  $V$  = 567.41(8) Å<sup>3</sup>,  $T$  = 295(2) K,  $Z$  = 2,  $\rho$  = 1.395 g cm<sup>-3</sup>,  $\mu$ (Mo-K $\alpha$ ) = 0.094 mm<sup>-1</sup>, reflections: 4774 collected, 2045 unique,  $R_{int}$  = 0.045,  $R_1$ (all) = 0.0618,  $wR_2$ (all) = 0.1587.

### Acknowledgements

This work was funded by the Fonds National de la Recherche Scientifique (FNRS) (PDR T.0102.15). We also thank the F.R.

S.-FNRS (Belgium) for a post-doctoral position allocated to D. A. S. We thank the COST action MP1202.

## References

- 1 C. Bertarellia, A. Biancoc, R. Castagnaa, G. Pariania and J. Photochem, *J. Photochem. Photobiol., C*, 2011, **12**, 106 and references therein.
- 2 P. Bamfield and M. G. Hutchings, *Technological Applications of Colour Chemistry, Chromic Phenomena*, Royal Society of Chemistry, Cambridge, 2010.
- 3 (a) M. Irie, *Chem. Rev.*, 2000, **100**, 1683; (b) S. Kobatake and M. Irie, *Annu. Rep. Prog. Chem., Sect. C: Phys. Chem.*, 2003, **99**, 277.
- 4 (a) E. Hadjoudis, M. Vitterakis, I. Moustakali and I. Mavridis, *Tetrahedron*, 1987, **43**, 1345; (b) E. Hadjoudis and I. M. Mavridis, *Chem. Soc. Rev.*, 2004, **33**, 579; (c) K. Amimoto and T. Kawato, *J. Photochem. Photobiol., C*, 2005, **6**, 207; (d) T. Haneda, M. Kawano, T. Kojima and M. Fujita, *Angew. Chem., Int. Ed.*, 2007, **46**, 6643; (e) E. Hadjoudis, S. D. Chatziefthimiou and I. M. Mavridis, *Curr. Org. Chem.*, 2009, **13**, 269; (f) Y. Inokuma, M. Kawano and M. Fujita, *Nat. Chem.*, 2011, **3**, 349.
- 5 (a) E. Hadjoudis, V. Verganelakis, C. Trapalis and G. Kordas, *Mol. Eng.*, 2000, **8**, 459; (b) F. Robert, A. D. Naik, B. Tinant, R. Robiette and Y. Garcia, *Chem. – Eur. J.*, 2009, **15**, 4327; (c) F. Robert, A. D. Naik and Y. Garcia, *J. Phys.: Conf. Ser.*, 2010, **217**, 012031; (d) Y. Garcia, F. Robert, A. D. Naik, G. Zhou, B. Tinant, K. Robeyns, S. Michotte and L. Piraux, *J. Am. Chem. Soc.*, 2011, **133**, 15850; (e) F. Robert, A. D. Naik, B. Tinant and Y. Garcia, *Inorg. Chim. Acta*, 2012, **380**, 104.
- 6 P.-L. Jacquemin, Y. Garcia and M. Devillers, *J. Mater. Chem. C*, 2014, **2**, 1815.
- 7 (a) F. Robert, A. D. Naik, F. Hidara, B. Tinant, R. Robiette, J. Wouters and Y. Garcia, *Eur. J. Org. Chem.*, 2010, 621; (b) F. Robert, P.-L. Jacquemin, B. Tinant and Y. Garcia, *CrystEngComm*, 2012, **14**, 4396; (c) D. A. Safin, K. Robeyns and Y. Garcia, *CrystEngComm*, 2012, **14**, 5523; (d) D. A. Safin, K. Robeyns and Y. Garcia, *RSC Adv.*, 2012, **2**, 11379.
- 8 (a) P.-L. Jacquemin, K. Robeyns, M. Devillers and Y. Garcia, *Chem. Commun.*, 2014, **50**, 649; (b) P.-L. Jacquemin, K. Robeyns, M. Devillers and Y. Garcia, *Chem. – Eur. J.*, 2015, **21**, 6832.
- 9 (a) R. Custelcean and J. E. Jackson, *Chem. Rev.*, 2001, **101**, 1963; (b) C. Schalley, *Introduction in Analytical Methods in Supramolecular Chemistry*, ed. C. Schalley, WILEY-VCH Verlag GmbH & Co. KGaA, Weinheim, 2007, pp. 1–16.
- 10 (a) M. S. M. Rawat and J. L. Norula, *Indian J. Chem., Sect. B: Org. Chem. Incl. Med. Chem.*, 1987, **26**, 232; (b) Y. Yildiz, Z. Kiliç and T. Hökelek, *J. Mol. Struct.*, 1988, **441**, 1; (c) N. Hoshino, T. Inabe, T. Mitani and Y. Maruyama, *Bull. Chem. Soc. Jpn.*, 1988, **61**, 4207; (d) T. Inabe, N. Hoshino, T. Mitani and Y. Maruyama, *Bull. Chem. Soc. Jpn.*, 1989, **62**, 2245; (e) E. Ito, H. Oji, T. Araki, K. Oichi, H. Ishii, Y. Ouchi, T. Ohta, N. Kosugi, Y. Maruyama, T. Naito, T. Inabe and K. Seki, *J. Am. Chem. Soc.*, 1997, **119**, 6336; (f) T. Sekikawa, T. Kobayashi and T. Inabe, *J. Phys. Chem. B*, 1997, **1**, 10645; (g) Z. Popović, V. Roje, G. Pavlović, D. Matković-Calogović and G. Giester, *J. Mol. Struct.*, 2001, **597**, 39; (h) E. Hadjoudis, A. Rontoyianni, K. Ambroziak, T. Dziembowska and I. Mavridis, *J. Photochem. Photobiol., A*, 2004, **162**, 521; (i) M. Taneda, K. Amimoto, H. Koyama and T. Kawato, *Org. Biomol. Chem.*, 2004, **1**, 499; (j) T. Fujiwara, J. Hadara and O. Keiichiro, *J. Phys. Chem. B*, 2004, **108**, 4035; (k) M. Ziólek, J. Kubicki, A. Maciejewski, R. Naskręcki and A. Grabowska, *J. Chem. Phys.*, 2006, **124**, 124518; (l) P. Xue, R. Lu, G. Chen, Y. Zhang, H. Nomoto, M. Takafuji and H. Ihara, *Chem. – Eur. J.*, 2007, **13**, 8231; (m) M. Taneda, H. Koyama and T. Kawato, *Chem. Lett.*, 2007, **36**, 354; (n) M. Ziólek, G. Burzinski and J. Karolczak, *J. Phys. Chem. A*, 2009, **113**, 2854; (o) P. Chen, R. Lu, P. Xue, T. Xu, G. Chen and Y. Zhao, *Langmuir*, 2009, **25**, 8395; (p) M. Taneda, H. Koyama and T. Kawato, *Res. Chem. Intermed.*, 2009, **35**, 643; (q) K. Tanaka, R. Shimoura and M. R. Caira, *Tetrahedron Lett.*, 2010, **51**, 449; (r) G. Ceyhan, M. Köse, V. McKee, S. Uru, A. Gölcü and M. Tümer, *Spectrochim. Acta*, 2012, **95**, 382; (s) D. A. Safin and Y. Garcia, *RSC Adv.*, 2013, **3**, 6466; (t) D. A. Safin, K. Robeyns, M. G. Babashkina, Y. Filinchuk, A. Rotaru, C. Jureschi, M. P. Mitoraj, J. Hooper, M. Brela and Y. Garcia, *CrystEngComm*, 2016, DOI: 10.1039/c6ce00266h.
- 11 (a) A. Rotaru, J. Dugay, R. P. Tan, I. Y. A. Gural'skiy, L. Salmon, P. Demont, J. Carrey, H. Molnar, M. Respaud and A. Bousseksou, *Adv. Mater.*, 2013, **25**, 1745; (b) C. Lefter, R. Tan, J. Dugay, S. Tricard, G. Molnar, L. Salmon, J. Carrey, A. Rotaru and A. Bousseksou, *Phys. Chem. Chem. Phys.*, 2015, **17**, 5151.
- 12 (a) Y. Garcia, P. J. van Koningsbruggen, E. Codjovi, R. Lapouyade, O. Kahn and L. Rabardel, *J. Mater. Chem.*, 1997, **7**, 857; (b) O. Kahn and C. J. Martinez, *Science*, 1998, **79**, 44.
- 13 (a) J. Linares, E. Codjovi and Y. Garcia, *Sensors*, 2012, **12**, 4479; (b) C. M. Jureschi, J. Linares, A. Rotaru, M. H. Ritti, M. Parlier, M. M. Dîrtu, M. Wolff and Y. Garcia, *Sensors*, 2015, **15**, 2388; (c) M. P. Cuellar, A. Lapresta-Fernandez, J. M. Herrera, A. Salinas-Castillo, M. C. Pegalajar, S. Titos-Padilla, E. Colacio and L. F. Capitan-Vallvey, *Sens. Actuators, B*, 2015, **208**, 180; (d) C. M. Jureschi, J. Linares, A. Boulmaali, P. R. Dahoo, A. Rotaru and Y. Garcia, *Sensors*, 2016, **16**, 187.
- 14 P. Gütllich, Y. Garcia and Th. Woike, *Coord. Chem. Rev.*, 2001, **219–221**, 839.
- 15 R. Herchel, L. Pavelek and Z. Travnicek, *Dalton Trans.*, 2011, **40**, 11896–11903.
- 16 (a) H. S. Scott, T. M. Ross, B. Moubaraki, K. S. Murray and S. M. Neville, *Eur. J. Inorg. Chem.*, 2013, 5–6, 803; (b) T. Wu, X.-P. Zhang, X.-Z. You, Y.-Z. Li and P. Bour, *ChemPlusChem*, 2014, **79**, 698.
- 17 M. A. Spackman and D. Jayatilaka, *CrystEngComm*, 2009, **11**, 19.
- 18 M. A. Spackman and J. J. McKinnon, *CrystEngComm*, 2002, **4**, 378.
- 19 S. K. Wolff, D. J. Grimwood, J. J. McKinnon, M. J. Turner, D. Jayatilaka and M. A. Spackman, *CrystalExplorer 3.1*, University of Western Australia, 2012.

- 20 C. Jelsch, K. Ejsmont and L. Huder, *IUCrJ*, 2014, **1**, 119.
- 21 V. A. Blatov, A. P. Shevchenko and D. M. Proserpio, *Cryst. Growth Des.*, 2014, **14**, 3576.
- 22 J. J. McKinnon, A. S. Mitchell and M. A. Spackman, *Chem. – Eur. J.*, 1998, **4**, 2136.
- 23 A. I. Kitaigorodsky, *Molecular Crystals and Molecules*, Academic Press, New York, 1973.
- 24 (a) D. A. Safin, M. P. Mitoraj, K. Robeyns, Y. Filinchuk and C. M. L. Vande Velde, *Dalton Trans.*, 2015, **44**, 16824; (b) M. G. Babashkina, K. Robeyns, Y. Filinchuk and D. A. Safin, *New J. Chem.*, 2016, **40**, 1230.
- 25 Rigaku Oxford Diffraction, *CrysAlisPro Software system*, Rigaku Corporation, Oxford, UK, 2014, Versions 1.171.35.19 and 1.171.37.35.
- 26 G. M. Sheldrick, *Acta Crystallogr., Sect. A: Found. Crystallogr.*, 2008, **64**, 112.
- 27 G. M. Sheldrick, *Acta Crystallogr., Sect. C: Struct. Chem.*, 2015, **71**, 3.
- 28 A. L. Spek, *Acta Crystallogr., Sect. D: Biol. Crystallogr.*, 2009, **65**, 148.
- 29 I. J. Bruno, J. C. Cole, P. R. Edgington, M. Kessler, C. F. Macrae, P. McCabe, J. Pearson and R. Taylor, *Acta Crystallogr., Sect. B: Struct. Sci.*, 2002, **58**, 389.